

X-RAY SPECTROSCOPY OF THE ACCRETING MILLISECOND PULSAR XTE J0929–314 IN OUTBURST

ADRIENNE M. JUETT¹, DUNCAN K. GALLOWAY, AND DEEPTO CHAKRABARTY^{1,2}

Center for Space Research, Massachusetts Institute of Technology, Cambridge, MA 02139;

ajuett, duncan, deepto@space.mit.edu

Accepted for publication in the *Astrophysical Journal*

ABSTRACT

We present the high-resolution spectrum of the accretion-powered millisecond pulsar XTE J0929–314 during its 2002 outburst, measured using the Low Energy Transmission Grating Spectrometer onboard the *Chandra X-ray Observatory*. The 1.5–25.3 Å (0.5–8.3 keV) *Chandra* spectrum is well fit by a power-law + blackbody model with photon index $\Gamma = 1.55 \pm 0.03$, blackbody temperature $kT_{\text{bb}} = 0.65 \pm 0.03$ keV, and blackbody normalization $R_{\text{bb,km}}/d_{10\text{kpc}} = 7.6 \pm 0.8$. No emission or absorption features are found in the high-resolution spectrum, with a 3σ equivalent width upper limit of < 0.007 Å at 1.5 Å and < 0.12 Å at 24 Å. The neutral absorption edge depths are consistent with the estimated interstellar absorption along the line of sight to the source. We found no orbital modulation of the 2–10 keV X-ray flux, to a 3σ upper limit of 1.1%, which implies an upper limit on the binary inclination angle of $i \lesssim 85^\circ$ for a Roche-lobe-filling companion. We also present the broadband spectrum measured over the course of the outburst by the *Rossi X-ray Timing Explorer (RXTE)*. The *RXTE* spectrum of XTE J0929–314 is also well fit with a power-law + blackbody model, with average values of $\Gamma = 1.76 \pm 0.03$, $kT_{\text{bb}} = 0.66 \pm 0.06$ keV, and $R_{\text{bb,km}}/d_{10\text{kpc}} = 5.9 \pm 1.3$ in the 2–50 keV energy range. The blackbody flux remained constant over the course of the outburst, while the power-law flux was strongly correlated to the (decreasing) flux of the source. We find that the difference in power-law photon indices measured from *Chandra* and *RXTE* spectra can be explained by a change in the power-law photon index at low energies.

Subject headings: binaries: close — stars: neutron — pulsars: individual (XTE J0929–314) — X-rays: binaries

1. INTRODUCTION

Millisecond pulsars (MSPs) have long been considered one of the possible endpoints of low-mass X-ray binary (LMXB) evolution. The neutron star (NS) is thought to be spun-up to a millisecond period by accretion from its low-mass companion. After the accretion phase has ended, the NS may turn on as a radio MSP. In the last five years, this theory has been confirmed with the identification of three accretion-powered MSPs, SAX J1808.4–3658, XTE J1751–305 and XTE J0929–314 (Wijnands & van der Klis 1998; Chakrabarty & Morgan 1998; Markwardt et al. 2002; Galloway et al. 2002).

Interestingly, all three accretion-powered MSPs are in short period binaries, with the two most recently discovered having binary periods ≈ 43 min (Markwardt et al. 2002; Galloway et al. 2002). These short periods place the MSPs XTE J1751–305 and XTE J0929–314 in the class of ultracompact binaries, defined as having orbital periods $\lesssim 80$ min. Ultracompact binaries require hydrogen-deficient or degenerate donors (Nelson, Rappaport, & Joss 1986). Recently, O and Ne emission and absorption features were discovered in two known and three suspected ultracompact systems (Schulz et al. 2001; Juett, Psaltis, & Chakrabarty 2001; Juett & Chakrabarty 2002). These results led the authors to conclude that the donor stars are degenerate C-O WDs. On the other hand, the *XMM-Newton* spectrum of XTE J1751–305 did not show emission or absorption features (Miller et al. 2002). In addition, no unusual abundances were required to fit the neutral absorption edges. This result is consistent with the suggestion of Markwardt et al. (2002) that the donor in XTE J1751–305 is a He WD (see also, Bildsten 2002).

XTE J0929–314 was discovered in April 2002 by the All

Sky Monitor onboard the *Rossi X-ray Timing Explorer (RXTE)*; Remillard 2002). Further *RXTE* observations detected 185 Hz pulsations modulated by a 43.6-min binary orbit (Remillard, Swank, & Strohmayer 2002; Galloway et al. 2002). Radio and optical counterparts with positions consistent with the X-ray position were also detected (Rupen, Dhawan, & Mioduszewski 2002; Greenhill, Giles, & Hill 2002; Cacella 2002). An optical spectrum of XTE J0929–314 revealed emission lines from C III/N III $\lambda 4640$ – 4650 and H α $\lambda 6563$ (Castro-Tirado et al. 2002). Given the optical detection of emission lines, and the ultracompact nature and high-Galactic latitude of the source, XTE J0929–314 is an ideal candidate for a high-resolution X-ray spectroscopic study to search for emission and absorption features similar to those seen in other ultracompact systems. In this letter, we present results from a Director’s Discretionary Time observation of XTE J0929–314 with the *Chandra X-ray Observatory*, as well as spectral results from the *RXTE* pointed observations throughout the outburst.

2. OBSERVATION AND DATA REDUCTION

The 2002 outburst of XTE J0929–314 began around MJD 52370 and peaked at ≈ 31 mCrab (2–10 keV) on MJD 52394 (Galloway et al. 2002). The pointed *RXTE* observations commenced 2 d later, and proceeded once every few days through MJD 52456. The source dropped below the 3σ detection limit of 7.5×10^{-12} erg cm⁻² s⁻¹ (2–10 keV; equivalent to 0.32 mCrab) after MJD 52443.

XTE J0929–314 was observed throughout its 2002 outburst by the two pointed instruments onboard *RXTE*. The Propor-

¹ Also Department of Physics, Massachusetts Institute of Technology, Cambridge, MA 02139

² Alfred P. Sloan Research Fellow

tional Counter Array (PCA; Jahoda et al. 1996) consists of five gas-filled proportional counter units (PCUs) with a total effective area of $\approx 6000 \text{ cm}^2$, sensitive to X-ray photons in the 2.5–60 keV range. The two instrument clusters comprising the High-Energy X-ray Timing Experiment (HEXTE; Gruber et al. 1996) present an effective area of $\approx 1600 \text{ cm}^2$ to photons in the energy range 15–250 keV. We extracted average spectra from standard instrument mode data (“Standard-2” and “Archive” for PCA and HEXTE, respectively) from each PCU/cluster for each observation. Since the instrumental gain is known to vary between PCUs, and also with time, we generated a separate response matrix for each PCU and each observation using `pcarsp` version 8.0, supplied with LHEASOFT version 5.2. We estimated background spectra using the “combined” gain epoch 5 (beginning 2000 May 13) faint-source model as input to `pcabackest` version 3.0. Over the course of the outburst, we collected 38 observations of XTE J0929–314 totaling 123.5 ks.

We also observed XTE J0929–314 with *Chandra* on 2002 May 15 (MJD 52409) for 18 ks using the Low Energy Transmission Grating Spectrometer (LETGS) and the Advanced CCD Imaging Spectrometer (ACIS; Weisskopf et al. 2002). The LETGS spectra are imaged by ACIS, an array of six CCD detectors. The LETGS/ACIS combination provides both an undispersed (zeroth order) image and dispersed spectra from the grating with a first order wavelength range of 1.4–63 Å (0.2–8.9 keV) and a spectral resolution of $\Delta\lambda = 0.05 \text{ Å}$. The various orders overlap and are sorted using the intrinsic energy resolution of the ACIS CCDs. The observation used a Y-offset of +1.5 in order to place the O-K absorption edge on the back-side illuminated S3 CCD, which has suffered less degradation than the front-side illuminated CCDs.

Using `tgdetect`, we determined the zeroth order source position of XTE J0929–314 to be: R.A.=09^h29^m20^s.15 and Dec.=−31°23′04″.3, equinox J2000.0 (90% confidence error of 0″.6³). The *Chandra* position is consistent with both the optical and radio counterpart positions (Rupen et al. 2002; Greenhill et al. 2002; Cacella 2002). The first order dispersed spectrum of XTE J0929–314 had an average count rate of $7.64 \pm 0.02 \text{ counts s}^{-1}$. We examined the total count rate, as well as the count rates in two different energy ranges, to check for changes in the spectral state. We found no evidence for any change of spectral state during the *Chandra* observation.

The “level 1” event file was processed using the CIAO v2.2 data analysis package⁴. The standard CIAO spectral reduction procedure was performed. We filtered the event file retaining those events tagged as afterglow events by the `acis_detect_afterglow` tool. Since order-sorting of grating spectra provides efficient rejection of background events, the afterglow detection tool is not necessary to detect cosmic ray afterglow events. No features were found that might be attributable to afterglow events.

For bright sources, pileup can be a problem for CCD detectors (see, e.g., Davis 2002). The zeroth order *Chandra* spectra of XTE J0929–314 was heavily affected by pileup and was not used in this analysis. In addition, it was found that the first order spectrum of XTE J0929–314 suffered from pileup in the range 5–12 Å (1–2.5 keV). In order to use the grating pileup kernel in ISIS, we created detector response files (ARFs) for each chip using the CIAO tool `mkgarf` and then combined

them to create +1 and −1 order ARFs using a custom tool developed by J. Davis of the HETGS instrument team. (This tool is similar to the standard CIAO tool but correctly calculates the fractional exposure at each response bin. This functionality has been added to the standard tools in CIAO v2.3.) The grating pileup kernel models the effect of pileup on grating spectra, similar to the pileup model available for CCD spectra in ISIS and XSPEC (see, Davis 2002, for a discussion of grating pileup modeling). In addition, the data and responses were rebinned to 0.083 Å to reflect the size of an ACIS event detection cell (3 CCD pixels). Background spectra were extracted from the standard LETG background regions. Spectral analysis of the *Chandra* observation of XTE J0929–314 was performed using ISIS (Houck & DeNicola 2000).

3. SEARCH FOR ORBITAL MODULATION

The presence (or absence) of orbital modulation of the X-ray flux can help constrain the inclination of the binary, and in turn the mass of the companion. Galloway et al. (2002) determined the orbital period of XTE J0929–314 to be 43.6 min from the Doppler modulation of the pulse arrival times. We searched both the *RXTE* and *Chandra* data for orbital modulation of the X-ray flux.

For the *RXTE* analysis, we calculated background-subtracted, solar-system barycenter corrected, 16-s binned lightcurves for each observation from photons in the energy range 3–13 keV. This range was selected to maximize the signal-to-noise ratio, and is identical to that used for the pulse timing analysis of Galloway et al. (2002). For each observation, we created a phase folded lightcurve of 8 bins using the measured orbital parameters, with phase zero set to the epoch of 90° mean longitude, $T_{\pi/2}$. The length of each observation was short compared to the decay timescale of the X-ray flux of XTE J0929–314, so it was not necessary to correct for the decline in X-ray flux during a single observation. Each lightcurve was then fit with a sine curve with variable amplitude and phase. From these results, we place a 3σ upper limit on the fractional rms modulation of 1.1%.

We also searched the *Chandra* data for orbital modulation of the X-ray flux. For the *Chandra* analysis, we first barycentered and randomized the first order grating events. Randomizing of the event arrival times consists of adding a random quantity uniformly distributed between 0–3.2 s, in order to avoid aliasing caused by the readout time. We calculated the phase of each first order event using the orbital parameters from Galloway et al. (2002) and created an 8 bin phase-folded lightcurve. We found an upper limit of 2.3% rms, consistent with the *RXTE* results.

Since the *Chandra* data is not subject to time gaps due to spacecraft motion, we also calculated a Fourier transform of the first order events which had been made into a 10-s binned lightcurve. We searched for modulations of the X-ray flux with frequencies between 6×10^{-5} and 5×10^{-2} Hz. We found no evidence for any periodic modulation, with a 90%-confidence upper limit of 1.4% for the fractional rms amplitude over the frequency range. The 90%-confidence upper limit for the fractional rms amplitude of a signal at the orbital period is 0.4%, well within the upper limits given by the phase folding analyses.

³ See <http://asc.harvard.edu/cal/ASPECT/celmon/index.html>

⁴ <http://asc.harvard.edu/ciao/>

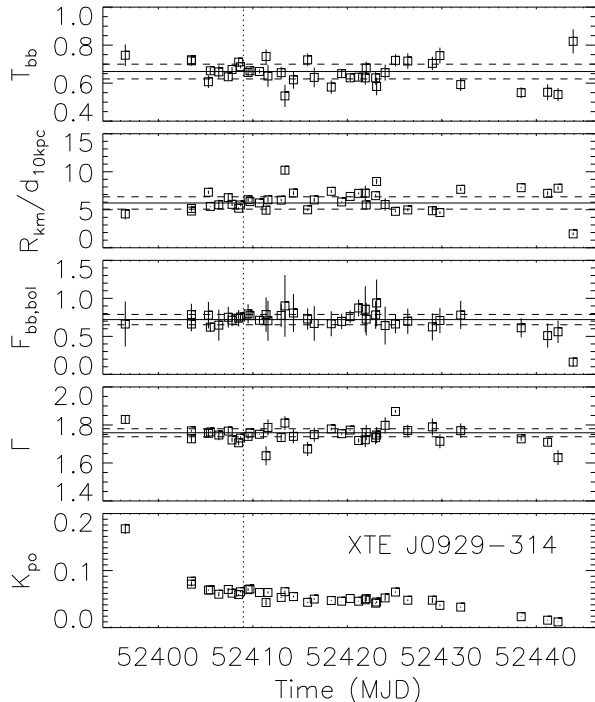


FIG. 1.— Spectral fit parameters derived from fitting an absorbed blackbody + power-law model to *RXTE* observations of XTE J0929–314. The panels, from top to bottom, show the blackbody temperature T_{bb} in keV; the blackbody normalization ($= R_{\text{bb,km}}/d_{10\text{kpc}}$), estimated bolometric flux of the blackbody component ($10^{-10} \text{ erg cm}^{-2} \text{ s}^{-1}$), power-law photon index Γ , and power-law normalization (photons $\text{keV}^{-1} \text{ cm}^{-2} \text{ s}^{-1}$ at 1 keV). The solid line shows the weighted mean over all the observations, while the dashed line shows the $\pm 1\sigma$ limits. The dotted line shows the time of the *Chandra* observation. Error bars show the 1σ uncertainties.

4. SPECTRAL ANALYSIS

4.1. *RXTE* Spectral Analysis

We fitted the combined 2–25 keV PCA and 15–50 keV HEXTE spectra with a number of models which typically give good fits for other X-ray pulsars, including broken and cut-off power laws and analytical Comptonization approximations. There was no evidence for a high-energy spectral cutoff within the energy range in which the source was detected (typically $\lesssim 50$ keV). We did however measure significant residuals below 10 keV. These residuals could be minimized by adopting a broken power law model where the spectral index decreased by $\approx 10\%$ (i.e. the spectrum became harder) above 7 keV, or by adding a blackbody component with $kT_{\text{bb}} \approx 0.5$ keV to a power law. While both these models gave fits of similar quality, we rejected the former as unphysical and instead adopted the latter for the remainder of the *RXTE* fits.

We also included a multiplicative component to take into account the attenuation by intervening (neutral) material with cosmic abundances. The equivalent hydrogen column density N_{H} exhibited no significant variations between observations, and in the mean was $\sim 10^{21} \text{ cm}^{-2}$, consistent with the line-of-sight values interpolated from dust and H I maps (7.6×10^{20} and 10^{21} cm^{-2} respectively; Schlegel, Finkbeiner, & Davis 1998; Dickey & Lockman 1990). For consistency with the fits to *Chandra* data, we froze the N_{H} value in subsequent fits at $7.6 \times 10^{20} \text{ cm}^{-2}$. The mean value of the reduced- χ^2 ($= \chi^2_{\nu}$) for

power-law + blackbody fits to spectra from all the observations was 1.04. While the worst-fitting observation gave a $\chi^2_{\nu} = 2.44$, the largest residuals arose from variations between PCUs (particularly at the lower energy bound) rather than any broad trend with energy. By excluding these lowest channels from the fit, and assuming a systematic error of 1%, we were able to reduce the fit statistic for that observation to $\chi^2_{\nu} = 1.30$.

The weighted mean of the blackbody temperature, kT_{bb} , was 0.66 ± 0.06 keV, while the normalization $\sqrt{K_{\text{bb}}} = R_{\text{bb,km}}/d_{10\text{kpc}} = 5.9 \pm 1.3$ (all errors are quoted at 90%-confidence unless otherwise noted). Both parameters showed variations during the outburst; however, they were significantly anticorrelated, so that the estimated bolometric blackbody flux ($\propto K_{\text{bb}} T_{\text{bb}}^4$) remained constant to within our measurement uncertainties ($\chi^2_{\nu} = 1.06$, see Figure 1). In the first observation, the blackbody component comprises only 3% of the flux in the 2–60 keV band, whereas in the last observation where significant blackbody and power-law components were detected, the blackbody accounted for 16% of the flux.

We calculated a weighted mean photon index of $\Gamma = 1.76 \pm 0.03$. The principal source of flux variation was the normalization of the power-law component (see Figure 1). While all parameters exhibited variations throughout the outburst, the power-law normalization was the only parameter to show a significant correlation with the integrated 2–10 keV flux (Spearman’s rank correlation coefficient $\rho = 0.908$, equivalent to 5.4σ ; Press et al. 1992). A power-law component was not significantly detected in the last observation on MJD 52443. A blackbody-only fit for that day exhibits a significantly (6.6σ) lower integrated blackbody flux than the weighted mean level for the previous observations. We did not detect XTE J0929–314 in subsequent observations (3σ upper limit on the 2–10 keV flux of $7.5 \times 10^{-12} \text{ erg cm}^{-2} \text{ s}^{-1}$).

4.2. *Chandra* Spectral Analysis

We fit the *Chandra* spectrum with a power-law + blackbody model including absorption. The +1.5 Y-offset in the observational setup allows for the entire 1.5–25.3 Å (0.5–8.3 keV) +1 order spectrum to be imaged on the S3 CCD. This CCD is backside-illuminated and has suffered less degradation than the front-side illuminated CCDs. Because of this and the lack of counts above 25 Å, we performed our spectral fits on only the +1 order spectrum in the range 1.5–25.3 Å.

Of the three known X-ray MSPs, XTE J0929–314 has the highest Galactic latitude and, probably the smallest interstellar column density along the line of sight to the source. Our *Chandra* observation allows for a direct determination of the strength of the absorption edges, in particular the O-K edge and the Fe-L triplet. To account for absorption and measure the optical depths of the edges, we used the *tbvarabs* absorption model (see, Wilms, Allen, & McCray 2000) with O and Fe abundances set to zero and the N_{H} fixed to $7.6 \times 10^{20} \text{ cm}^{-2}$, the hydrogen column from dust maps (Schlegel et al. 1998). The O edge was fit with an edge model, while the Fe-L edges were fit using a custom model that employs the optical constant measurements of Kortricht & Kim (2000). In addition, the C abundance in *tbvarabs* was allowed to vary in order to account for the known instrumental contamination of the ACIS CCDs⁵ (Plucinsky et al. 2002). We also included Gaussian lines to fit the interstellar atomic O absorption line at 23.5 Å and the absorption feature

⁵ For more information see, http://cxc.harvard.edu/cal/Links/Acis/acis/Cal_prods/qeDeg/index.html

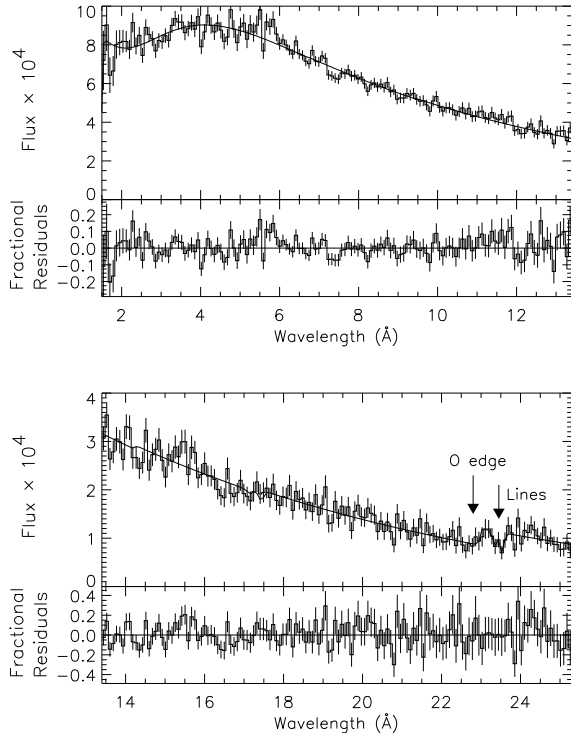


FIG. 2.— (*upper panels*) *Chandra* LETG +1 order flux spectrum (in units of photons $\text{cm}^{-2} \text{s}^{-1} \text{\AA}^{-1}$) of XTE J0929–314 with best-fit power-law + blackbody model with absorption. The arrows indicate the positions of the O edge, and the atomic O and Fe_2O_3 absorption lines. (*lower panels*) Fractional residuals ($[\text{data} - \text{model}]/\text{model}$) of the LETG spectral fit shown above. The absorption models are consistent with the predicted interstellar absorption from dust maps.

at 23.36\AA , attributed to a $1s\text{-}2p$ transition in Fe_2O_3 (see, Schulz et al. 2002).

We found a best-fit photon index of 1.55 ± 0.03 , with a normalization of $(4.04 \pm 0.15) \times 10^{-2}$ photons $\text{keV}^{-1} \text{cm}^{-2} \text{s}^{-1}$ at 1 keV. The *Chandra* best-fit blackbody temperature was $kT_{\text{bb}} = 0.65 \pm 0.03$ keV, with $R_{\text{bb,km}}/d_{10\text{kpc}} = 7.6 \pm 0.8$. Our best-fit model had a $\chi^2_{\nu} = 1.001$ and an unabsorbed 2–10 keV flux of 2.7×10^{-10} erg $\text{cm}^{-2} \text{s}^{-1}$.

The best-fit optical depth for O was 0.34 ± 0.07 , which translates to an equivalent hydrogen column density of $(1.2 \pm 0.3) \times 10^{21} \text{cm}^{-2}$, using the cross-section of Henke, Gullikson, & Davis (1993) and the O ISM abundance of Wilms et al. (2000). Although this is somewhat higher than the measured hydrogen column from dust maps, an instrumental contribution to the O edge has been reported, with an optical depth of ≈ 0.10 (Plucinsky et al. 2002). This contribution would add $N_{\text{H}} \approx 0.36 \times 10^{21} \text{cm}^{-2}$ to the expected value, making the *Chandra* O edge measurement compatible with the dust map measurement. The best-fit line wavelength and equivalent width (EW) of the atomic O absorption line were $23.52 \pm 0.05 \text{\AA}$ and $0.053^{+0.005}_{-0.03} \text{\AA}$. The Fe_2O_3 absorption line and Fe-L edges were not significantly detected, with an upper limit on the Fe column density of $3 \times 10^{16} \text{cm}^{-2}$, equivalent to an $N_{\text{H}} < 1.1 \times 10^{21} \text{cm}^{-2}$. The best-fit C abundance was $7.8^{+1.2}_{-0.7}$ times the interstellar C/H ratio of Wilms et al. (2000). This is slightly lower than the expected instrumental + interstellar contribution of 9.9 ± 0.5 times the interstellar ratio. The instrumental edge depths for C and O were estimated using the recent calibration results presented at

the *Chandra X-ray Center* website⁵ (see also, Plucinsky et al. 2002).

Besides the interstellar O absorption line, there were no prominent emission or absorption lines in the high-resolution spectrum of XTE J0929–314 (see Figure 2). We performed a careful search of the *Chandra* spectral residuals to place limits on the presence of any spectral features. Gaussian models with fixed $\text{FWHM} = 2000 \text{km s}^{-1}$ were fit at each point in the wavelength range $1.5\text{--}25.3 \text{\AA}$. From this, we can place a 3σ upper limit on the EW of any line feature, either emission or absorption. The EW limit increases approximately linearly with wavelength, varying from 0.007\AA at 1.5\AA to 0.12\AA at 24\AA .

Our measured C abundance depends on the assumed continuum model since the edge depth can not be directly measured (the C edge at 43\AA is outside our bandpass). In order to test if the C abundance was the cause of the difference in the photon index between the *Chandra* and *RXTE* fits, we refit the *Chandra* spectrum with a fixed C abundance of 9.9 times the interstellar C/H ratio. With the C abundance fixed, the best-fit photon index was 1.62 ± 0.03 . This is still significantly different from the best-fit photon index found in the *RXTE* spectra. The best-fit power-law normalization increased to $(4.50 \pm 0.07) \times 10^{-2}$ photons $\text{keV}^{-1} \text{cm}^{-2} \text{s}^{-1}$. The other fit parameters were consistent with the previous fit within errors. We also considered the possibility that the pileup model was giving rise to the lower photon index in the *Chandra* spectral fits. When the *Chandra* data is fit without the pileup model, and excluding the piled-up region (1–3 keV) of the spectrum, we find spectral parameters consistent with the results found using the pileup model.

5. COMBINED *Chandra* AND *RXTE* SPECTRAL FITS

To investigate the difference in the spectral results between *Chandra* and *RXTE*, we performed combined spectral fits with the *Chandra* and *RXTE* data. A single *RXTE* observation (70096-03-05-00), taken within a few hours of the *Chandra* data, was used to represent the *RXTE* spectrum of XTE J0929–314. To simplify fitting, the piled-up region (1–3 keV) of the *Chandra* data was excluded and the pileup kernel was not used. The combined data were fit with a blackbody + either a power-law, broken power-law or the `comptt` model which describes Comptonization of soft photons by a hot plasma (Titarchuk 1994). The broken power-law and Comptonization models allow for turnover at low energies which could explain the difference in the *Chandra* and *RXTE* spectral results. The absorption was described by the `tbvarabs` model with the C abundance allowed to vary for the *Chandra* observation only, while best-fit edge depths from the *Chandra* analysis were used for the O and Fe edges. We also included a Gaussian line, fixed to the best-fit *Chandra* value, to model the atomic O absorption at 23.5\AA . Multiplicative constants were included to compensate for any instrumental normalization differences. We find that the normalizations of the PCA spectra are $\approx 20\%$ larger than for *Chandra*, while the HEXTE spectra are $\approx 20\%$ lower. Similar normalization differences have been noted before (see, e.g., Kuulkers et al. 2002, and references therein).

As a check on the instrumental calibrations, we directly compared the *Chandra* and *RXTE* data in the same energy range by fitting the high energy (3–8 keV) *Chandra* data, in conjunction with the *RXTE* data, to an absorbed power-law + blackbody model with absorption fixed to $N_{\text{H}} = 7.6 \times 10^{20} \text{cm}^{-2}$. The fits are consistent with the results of the *RXTE* data, $\Gamma = 1.74 \pm$

0.02, $kT_{\text{bb}} = 0.66 \pm 0.03$ keV, and $R_{\text{bb,km}}/d_{10\text{kpc}} = 5.9 \pm 0.7$, with $\chi^2_{\nu} = 1.03$.

We then fit the full *Chandra* and *RXTE* spectra with a power-law + blackbody model. When the edge parameters were fixed to the *Chandra* best-fit values, the photon index had a best-fit value of 1.628 ± 0.009 and with a $\chi^2_{\nu} = 1.20$ (see Table 1). We note that the χ^2_{ν} of the power-law + blackbody fit to the *RXTE* data alone was 1.06. If we fix the C abundance to the expected value of 9.9 times the interstellar C/H ratio, the photon index increases to 1.656 ± 0.009 ($\chi^2_{\nu} = 1.14$). If we instead allow the C abundance to vary, the best-fit photon index increases to 1.72 ± 0.02 ($\chi^2_{\nu} = 1.09$), giving a photon index consistent with the *RXTE* spectral results, but with a C abundance of 14.1 ± 1.2 times the interstellar C/H ratio. This value is inconsistent with the estimate of the C abundance from instrument calibration work (see §4.2). As can be seen, the continuum spectral parameters are highly dependent on the assumed absorption.

We performed the same fits using the `comptt` in place of the power-law component. The Comptonization model provides for a low-energy turnover in the spectrum. The electron temperature was fixed to 50 keV, the upper limit of the energy range. In addition, we used a spherical geometry in order to compare with the spectral fit of SAX J1808.4–3658 (Titarchuk, Cui, Wood 2002). The `comptt` model provides a better fit to the data compared with the power-law ($\chi^2_{\nu} = 1.09$ – 1.07 , see Table 1). We performed an *F*-test to formally compare the two models and found that in all cases the Comptonization model was better with a significance $> 99\%$. For the two fixed values of the C abundance, the results of the `comptt` + blackbody fits are consistent within error with a seed photon temperature, $kT_0 \approx 0.13$ keV and optical depth, $\tau_p \approx 2.7$. When the C abundance is allowed to vary, the fit improves but becomes inconsistent with the other results, which is probably due to degeneracy between the parameters.

In the best-fit `comptt` + blackbody model, the blackbody component has parameter values of $kT_{\text{bb}} = 0.71$ keV and $R_{\text{bb,km}}/d_{10\text{kpc}} = 5.5$. These values are consistent with the power-law fits both to the combined data and with the blackbody parameters from each instrument fit, indicating that the blackbody temperature and flux are independent of the exact continuum model used. We find $kT_0 < kT_{\text{bb}}$, similar to the fit of

SAX J1808.4–3658 using the same model (Titarchuk et al. 2002). We note that the `comptt` model is in itself an approximation to a full treatment of Comptonization, in particular at soft energies. If we assume that the blackbody provides the input photons to the Comptonization component, then we would expect $kT_0 = kT_{\text{bb}}$. We fit the data with the constraint $kT_0 = kT_{\text{bb}}$, but the fit was unreasonable with $\chi^2_{\nu} > 2.0$. Interestingly, Gierliński, Done, & Barret (2002) used a different Comptonization model and found $kT_0 = kT_{\text{bb}}$ in spectral fits of SAX J1808.4–3658. We employed the same model to fit XTE J0929–314 (`compPS`; Poutanen & Svensson 1996), but found similar values for the input photon temperature and optical depth as found using the `comptt` model.

We also fit the data with a broken power-law + blackbody model to test for low-energy turnover without relying on the assumptions inherent in the Comptonization model. We find that the data is also well fit ($\chi^2_{\nu} = 1.08$) by a broken power-law + blackbody model with $\Gamma_1 = 1.26$ – 1.56 , $\Gamma_2 = 1.75$, and $E_{\text{break}} = 1.4$ – 4.4 keV, and blackbody parameters consistent with previous fits (see Table 1).

6. DISCUSSION

We have found that the spectrum of XTE J0929–314 is well described by a power-law + blackbody model over limited energy ranges, with interstellar absorption consistent with $N_{\text{H}} = 7.6 \times 10^{20}$ cm $^{-2}$, the expected hydrogen column density along the line of sight to the source. The *Chandra* spectrum shows no prominent emission or absorption lines in the spectrum (similar to XTE J1751–305; Miller et al. 2002), with an EW limit which varies from < 0.007 Å at 1.5 Å to < 0.12 Å at 24 Å. No orbital modulation of the X-ray flux was detected in either the *Chandra* or *RXTE* data. From the lack of X-ray eclipses, we set an upper limit on the binary inclination of $i \lesssim 85^\circ$ for a Roche-lobe–filling companion. In addition, the absence of dips in the X-ray lightcurve suggests that the source is most likely at an inclination of $i \lesssim 60^\circ$ – 70° (see, e.g., Frank, King, & Lasota 1987; White, Nagase, & Parmar 1995).

The blackbody spectral component in LMXBs is generally attributed to the neutron star, possibly from a “hot spot” where the accretion column meets the neutron star surface. From our

TABLE 1
COMBINED *Chandra* AND *RXTE* SPECTRAL FITS^a

Model	Carbon Abundance ^b	Γ_1/kT_0 (keV)	E_{break} (keV)	Γ_2/τ	$K_{\text{po}}/K_{\text{Comp}}^c$	kT_{bb} (keV)	$R_{\text{km}}/d_{10\text{kpc}}$	χ^2/dof
PL	7.8 (fix)	1.628 ± 0.009	4.58 ± 0.07	0.730 ± 0.015	5.3 ± 0.3	1006/837
PL	9.9 (fix)	1.656 ± 0.009	4.90 ± 0.08	0.717 ± 0.016	5.3 ± 0.3	950/837
PL	14.1 ± 1.2	1.72 ± 0.02	5.7 ± 0.3	0.68 ± 0.02	5.6 ± 0.4	904/833
Comp	7.8 (fix)	0.144 ± 0.009	...	2.72 ± 0.06	3.21 ± 0.09	0.709 ± 0.016	5.4 ± 0.3	911/836
Comp	9.9 (fix)	0.125 ± 0.014	...	2.69 ± 0.06	3.6 ± 0.2	0.707 ± 0.017	5.5 ± 0.4	906/836
Comp	13.2 ± 1.2	$0.07^{+0.04}_{-0.07}$...	2.55 ± 0.07	$5.8^{+7.5}_{-1.8}$	0.67 ± 0.02	5.8 ± 0.4	894/832
BKN PL	7.8 (fix)	1.26 ± 0.09	1.4 ± 0.3	1.74 ± 0.02	5.06 ± 0.19	0.66 ± 0.03	5.8 ± 0.7	900/835
BKN PL	9.9 (fix)	1.56 ± 0.03	4.4 ± 0.9	1.75 ± 0.02	4.67 ± 0.17	0.61 ± 0.03	7.7 ± 1.9	897/835

^aAll errors are quoted at the 90%-confidence level

^bCarbon abundance ratio relative to ISM, $(\text{C}/\text{H})/(\text{C}/\text{H})_{\text{ISM}}$

^cPower-law and broken power-law normalization at 1 keV in units of 10^{-2} photons keV $^{-1}$ cm $^{-2}$ s $^{-1}$. Comptonization normalization in units of 10^{-3} .

fits, we find a blackbody radius of $R_{\text{bb,km}} = (5.3 - 7.7) d_{10\text{kpc}}$. Given the lower limit on the distance of 5 kpc (Galloway et al. 2002), we find a lower limit on the blackbody radius of $R_{\text{bb}} > 2.7$ km. We note that this lower limit does not include a correction for the conversion between the color temperature and the effective temperature of the neutron star atmosphere (see, Lewin, van Paradijs, & Taam 1993, for a discussion). This correction could increase the inferred radius by a factor of ≈ 2 . But even after this correction, the inferred radius is not consistent with canonical NS models for a distance of 5 kpc suggesting a “hot spot” emission region.

During the outburst, we found that the blackbody flux remained constant, while the power-law flux declined. In addition, when the combined *Chandra* and *RXTE* spectrum is fit with a Comptonization model, we find that the blackbody temperature, kT_{bb} , is significantly greater than the seed photon temperature of the Comptonization model, kT_0 . This evidence suggests that the power-law and blackbody components are associated with different emission processes.

We compared our results with two physical models that were developed to explain the spectral properties of the accretion-powered MSP SAX J1808.4–3658 (Gierliński et al. 2002; Titarchuk et al. 2002). Both models were formulated using data from the 1998 outburst of SAX J1808.4–3658, but come to very different conclusions regarding the relationship between the power-law or Comptonization component and the blackbody. Gierliński et al. (2002) assumed that the blackbody was the source of the seed photons (i.e., $kT_0 = kT_{\text{bb}}$) and proposed that the Comptonization component comes from the shock heated accretion column with soft photon input from the “hot spot” blackbody component. Such a model implies that the blackbody and power-law/Comptonization component fluxes should be correlated, which was the case for SAX J1808.4–3658 but was not seen for XTE J0929–314.

On the other hand, Titarchuk et al. (2002) found that $kT_0 \ll kT_{\text{bb}}$ and suggested that the accretion disk provided the majority of the soft photon input to a spherical Compton cloud, of radius $R \approx 60$ km, from which the Comptonization component originates. The Titarchuk et al. (2002) model allows for the blackbody and power-law/Comptonization component to vary independently. Titarchuk et al. (2002) also suggested that the low ($\tau_0 \approx 4$) optical depth of the Comptonizing region found for SAX J1808.4–3658 allows for the pulsations of the NS to be detected, while the higher optical depths ($\tau_0 > 5$) reported in more luminous LMXBs suppress the pulsation amplitudes. We find a best-fit $\tau_0 \approx 2.7$ for XTE J0929–314, consistent with this explanation. However, we note that Miller et al. (2002) did not find an acceptable fit of the *XMM* spectra of the millisecond X-ray pulsar XTE J1751–305 using a Comptonization model. While this model seems more appropriate for the spectral results of XTE J0929–314, Titarchuk et al. (2002) do not discuss what emission component is responsible for the pulsations.

It is important to realize that both models are based on data with a low-energy bound of 2 keV, which is above the peak flux of the thermal components. The lower energy range of *Chan-*

dra allows us to make a more robust measurement of kT_0 for XTE J0929–314 than was possible for the *RXTE* spectrum of SAX J1808.4–3658. We conclude that neither model is completely appropriate to explain both our results. More observations of these sources throughout outburst are necessary in order to fully understand their phase-averaged spectral properties. We suggest that in-depth data analysis, including pulse-phase spectroscopy, will provide more insight into the relationship between the various spectral components. The pulse-phase resolved spectral analysis of XTE J0929–314 will be presented in a later paper.

We find that the best-fit photon index was significantly different between the *Chandra* and *RXTE* fits with $\Gamma = 1.55 - 1.62$ for the *Chandra* fits, dependent on the assumed instrumental C abundance, and $\Gamma = 1.76$ for the *RXTE* fits. Since fits with and without the pileup model give consistent parameter values, we reject the possibility that pileup causes the lower *Chandra* photon index. The combined *Chandra* and *RXTE* spectrum of XTE J0929–314 is well fit by either a Comptonization + blackbody model (which implicitly includes a low-energy turnover from the Comptonization component), or a broken power-law + blackbody model, with break energy 1.4–4.4 keV. The high-energy ($E > 3$ keV) *Chandra* spectrum is consistent with the *RXTE* spectral results, indicating that instrumental differences alone do not give rise to the spectral turnover. Based on these results, we suggest that the difference in best-fit photon indices between *Chandra* and *RXTE* arises from spectral turnover at low energies. While a power-law model is a reasonable approximation to Comptonization at high energies, extrapolating the power law to low energies leads to a predicted flux that diverges at zero energy. Therefore, the power-law must turnover at some energy for the integrated flux to be finite.

In addition, the difference in the photon index between the *Chandra* and *RXTE* spectral fits is similar to that noted by Miller et al. (2002) between the *RXTE* and *XMM* spectral fits of XTE J1751–305. From their *XMM* EPIC spectrum, Miller et al. (2002) found a best-fit power-law photon index of 1.44, while Markwardt et al. (2002) found a best-fit photon index of 1.7–1.9 using *RXTE*. We interpret the difference between the *XMM* and *RXTE* spectral results for XTE J1751–305 as evidence of low energy turnover in the broadband spectrum of that source, providing independent support that the turnover is astrophysical in origin.

We would like to thank *Chandra* Director Harvey Tananbaum and *RXTE* Director Jean Swank for approving our DDT/TOO observations. In addition, we acknowledge useful discussions with Craig Markwardt, Jon Miller, Mike Nowak, and Dimitrios Psaltis. This research has made use of data obtained through the High Energy Astrophysics Science Archive Research Center Online Service, provided by the NASA/Goddard Space Flight Center. This work was supported in part by NASA under contract NAS8-01129 and grant NAG5-9184.

REFERENCES

- Bildsten, L. 2002, ApJ, 577, L27
 Cacella, P. 2002, IAU Circ., No. 7893
 Castro-Tirado, A. J., Caccianiga, A., Gorosabel, J., Kilmartin, P., Tristram, P., Yock, P., Sanchez-Fernandez, C., & Alcoholado-Felstrom, M. E. 2002, IAU Circ., No. 7895
 Chakrabarty, D. & Morgan, E. H. 1998, Nature, 394, 346
 Davis, J. 2002, Proc. SPIE, submitted
 Dickey, J. M. & Lockman, F. J. 1990, ARA&A, 28, 215
 Frank, J., King, A. R., & Lasota, J.-P. 1987, A&A, 178, 137
 Galloway, D. K., Chakrabarty, D., Morgan, E. H., & Remillard, R. A. 2002, ApJ, 576, L137
 Gierliński, M., Done, C., & Barret, D. 2002, MNRAS, 331, 141

- Greenhill, J. G., Giles, A. B., & Hill, K. M. 2002, IAU Circ., No. 7889
- Gruber, D. E., Blanco, P. R., Heindl, W. A., Pelling, M. R., Rothschild, R. E., & Hink, P. L. 1996, *A&AS*, 120, C641
- Henke, B. L., Gullikson, E. M., & Davis, J. C. 1993, *Atomic Data & Nucl. Data Tables*, 54, 181
- Houck, J. C., & DeNicola, L. A. 2000, in *ASP Conf. Ser. 216, Astronomical Data Analysis Software and Systems IX*, ed. N. Manset, C. Veillet, & D. Crabtree (San Francisco: ASP), 591
- Jahoda, K., Swank, J. H., Giles, A. B., Stark, M. J., Strohmayer, T., Zhang, W., & Morgan, E. H. 1996, *Proc. SPIE*, 2808, 59
- Juett, A. M. & Chakrabarty, D. 2002, *ApJ*, submitted (astro-ph/0206417)
- Juett, A. M., Psaltis, D., & Chakrabarty, D. 2001, *ApJ*, 560, L59
- Kortright, J. B., & Kim, S.-K. 2000, *Phys. Rev. B*, 62, 12216
- Kuulkers, E., den Hartog, P. R., in 't Zand, J. J. M., Verbunt, F. W. M., Harris, W. E., & Cocchi, M. 2002, *A&A*, accepted (astro-ph/0212028)
- Lewin, W. H. G., van Paradijs, J., & Taam, R. E. 1993, *SSRv*, 62, 223
- Markwardt, C. B., Swank, J. H., Strohmayer, T. E., in 't Zand, J. J. M., & Marshall, F. E. 2002, *ApJ*, 575, L21
- Miller, J. M., Wijnands, R., Méndez, M., Tiengo, A., van der Klis, M., Chakrabarty, D., Gaensler, B. M., & Lewin, W. H. G. 2002, *ApJ*, submitted (astro-ph/0208166)
- Nelson, L. A., Rappaport, S. A., & Joss, P. C. 1986, *ApJ*, 304, 231
- Plucinsky, P. P. et al. 2002, *Proc. SPIE*, 4851, in press (astro-ph/0209161)
- Poutanen, J. & Svensson, R., 1996, *ApJ*, 470, 249
- Press, W. H., Teukolsky, S. A., Vetterling, W. T., & Flannery, B. P. 1992, *Numerical recipes in FORTRAN. The art of scientific computing* (2nd ed.; New York: Cambridge University Press)
- Remillard, R. A. 2002, IAU Circ., No. 7893
- Remillard, R. A., Swank, J., & Strohmayer, T. 2002, IAU Circ., No. 7893
- Rupen, M. P., Dhawan, V., & Mioduszewski, A. J. 2002, IAU Circ., No. 7893
- Schlegel, D. J., Finkbeiner, D. P., & Davis, M. 1998, *ApJ*, 500, 525
- Schulz, N. S., Chakrabarty, D., Marshall, H. L., Canizares, C. R., Lee, J. C., & Houck, J. 2001, *ApJ*, 563, 941
- Schulz, N. S., Cui, W., Canizares, C. R., Marshall, H. L., Lee, J. C., Miller, J. M., & Lewin, W. H. G. 2002, *ApJ*, 565, 1141
- Titarchuk, L. 1994, *ApJ*, 434, 313
- Titarchuk, L., Cui, W., & Wood, K. 2002, *ApJ*, 576, L49
- Weisskopf, M. C., Brinkman, B., Canizares, C., Garmire, G., Murray, S., & van Speybroeck, L. P. 2002, *PASP*, 114, 1
- White, N. E., Nagase, F., & Parmar, A. N. 1995, in *X-ray Binaries*, ed. W. H. G. Lewin, J. van Paradijs, & E. P. J. van den Heuvel (Cambridge: Cambridge Univ. Press), 1
- Wijnands, R. & van der Klis, M. 1998, 394, 344
- Wilms, J., Allen, A., & McCray, R. 2000, *ApJ*, 542, 914